THE ASTROPHYSICAL JOURNAL, 284:223–237, 1984 September 1

CARBON, NITROGEN, AND OXYGEN ABUNDANCES IN BETELGEUSE

DAVID L. LAMBERT[1] AND JEFFERY A. BROWN
Department of Astronomy, University of Texas
KENNETH H. HINKLE
Kitt Peak National Observatory[2]
AND
HOLLIS R. JOHNSON
Astronomy Department, Indiana University
Received 1983 April 14; accepted 1984 March 12

ABSTRACT

Vibration-rotation bands of CO, NH, and OH and infrared lines of the CN red system in the spectrum of the M supergiant Betelgeuse (α Orionis) are analyzed to obtain the C, N, and O abundances. A model atmosphere with $T_{\rm eff} = 3800$ K and $\log g = 0.0$ is adopted. Results are:

$$\log \epsilon(\mathrm{C}) = 8.4\,, \qquad \log \epsilon(\mathrm{N}) = 8.6\,, \qquad \text{and} \qquad \log \epsilon(\mathrm{O}) = 8.8\,.$$

If α Ori is assumed to be metal rich by about 0.1 dex, the atmosphere compared with that of an unevolved star is deficient in ^{12}C, and richer in ^{14}N:

$$[\mathrm{C}] = -0.4\,, \qquad [\mathrm{N}] = +0.6\,, \qquad \text{and} \qquad [\mathrm{O}] = -0.2\,.$$

These abundances and especially the low C/N ratio ([C/N] = −0.9) with the low ^{12}C/^{13}C ratio suggest that CN-cycle processed material has been mixed to the surface as a result of the first dredge-up phase. With the exception of the observed high ^{13}C abundances, the observed and predicted abundances are in good agreement. This analysis does not confirm recent reports that C is severely underabundant.

Subject headings: nucleosynthesis — stars: abundances — stars: individual — stars: interiors — stars: supergiants

I. INTRODUCTION

The atmosphere of a red giant contains material processed by nuclear reactions in the interior and mixed out to the surface. In this paper, we discuss the elemental abundances of C, N, and O for the M supergiant Betelgeuse (α Ori) and try to trace the origin of the processed material in the atmosphere.

Abundance analyses for the M supergiants are rare in the literature. The initial attempt at a CNO analysis was reported by Spinrad and Vardya (1966). We restrict discussion to their results for α Ori. They observed bands of H_2, H_2O, CN, and CO and analyzed the molecular column densities with crude model atmospheres. The C abundance was reported to be enhanced (i.e., O/C = 1.05, where O/C = 1.6 for the Sun) and accompanied by a stronger enhancement of N (i.e., N/C ≈ N/O = 2 whereas N/O ≈ 0.1 for the Sun). The O abundance was found to be nearly solar. However, new infrared spectra reduced the CO column density (Spinrad *et al.* 1970) by a factor of 15. Then, the features assigned to H_2O were identified with CN red system bands (Wing and Spinrad 1970) and the original identifications of H_2 were rejected by Lambert, Brooke, and Barnes (1973). Clearly, this initial analysis must be discarded. Spectra in the 3–4 μm window provided Beer *et al.* (1972) with lines of the fundamental vibration-rotation (V-R) bands of OH. The OH column density was derived and compared with predictions (Goon and Auman 1970) obtained from model atmospheres (Auman 1969). Beer *et al.* suggested that both C (here the CO column density was used) and O were underabundant by about a factor of 10 relative to solar abundances. Unfortunately, the OH and CO lines used by Beer *et al.* are strong so that the column density is sensitive to the assumed microturbulence. High-resolution observations of portions of the 5 μm fundamental V-R bands of CO were analyzed by Geballe *et al.* (1977) who concluded that the C/H ratio was about a factor of 12 smaller than the solar ratio. A recent model atmosphere analysis of CO, OH, and CN lines led to a severe depletion of C, an enhancement of N and a near-solar abundance of O (Tsuji 1979). Jura and Morris (1981), who modeled the K I 7699 Å fluorescent emission and the CO rotational line emission from the circumstellar shell, suggested that C in the shell and, hence, in the stellar photosphere was deficient by a factor of about 25.

Our analysis was stimulated, in part, by an earlier preliminary analysis of weak CO second-overtone V-R lines which showed that, in contrast to a majority of the earlier analyses, carbon was not strongly depleted in the atmosphere (Lambert 1974). A new comprehensive analysis was begun in an attempt to resolve these conflicting reports. Our attack on the CNO abundances uses line-blanketed model atmospheres for M supergiants. We consider several indicators of the CNO abundances; the primary sources are the following molecular transitions: the CO second overtone V-R bands near 1.6 μm, the NH fundamental V-R 1–0 and 2–1 bands between 3 and 4 μm, the OH fundamental V-R bands also near 3 μm and lines near 2 μm of the CN red system. We also discuss the [O I] lines and the CN red system lines at 8000 Å.

Our model atmospheres and the defining parameters are

[1] John Simon Guggenheim Memorial Fellow, 1980–1981.
[2] KPNO is operated by the Association Universities for Research in Astronomy, Inc., under contract with the National Science Foundation.

discussed in § II. After a brief discussion of the observations (§ III), we present the abundance analysis in § IV and conclude (§ V) with a discussion of the abundances and the predictions of nucleosynthesis and mixing in red supergiants.

II. MODEL ATMOSPHERES

a) Description of the Models

Realistic model atmospheres for cool giant and supergiant stars are now available in quantity. Interested readers should refer for details to the original papers (Gustafsson *et al.* 1975; Tsuji 1976*a*; Johnson, Bernat, and Krupp 1980, hereafter JBK).

Our model atmospheres are taken from the JBK grid of red giant models or were computed from the same code specifically for this project. The input defining parameters are the effective temperature ($T_{\rm eff}$), the surface gravity (g), and the chemical composition. The models are subject to the conventional principles of theoretical stellar atmospheres. These principles include the equation of hydrostatic equilibrium, constancy of total energy flux (radiative and convective) and local thermodynamic equilibrium in a plane-parallel, horizontally homogeneous geometry. The pressure term in the equation of hydrostatic equilibrium includes gas and radiation pressure, but turbulent pressure was neglected except for two models with 2 and 3 km s^{-1}. The assumption of a plane-parallel atmosphere for a supergiant such as Betelgeuse will be discussed later. Convection is treated with the standard mixing-length theory (see, for example, Kurucz 1970), and the ratio of mixing length to pressure scale height is taken as unity. The set of equations is quite standard and has already been repeatedly discussed in the literature. The equations outlined above are solved by the model stellar atmosphere program ATLAS5 (Kurucz 1970), which is also well known, thoroughly described, and often used.

Most of our models have solar composition but a few additional models have enhanced metal abundances. The JBK paper contains information relating to ionization energies, dissociation energies, and line and band strengths. The code accounts for the line opacity of many atoms as well as lines of the molecules CO, CN, C_2, TiO, NH, MgH, OH, and H_2O. The standard hydrogen and helium opacity of ATLAS5 are included as described by Kurucz (1970).

All of these lines except those of H_2O were treated by the opacity sampling technique, which has been described by Peytremann (1974), Sneden, Johnson, and Krupp (1974), and Johnson and Krupp (1976) and has been used in calculations of a wide variety of stellar atmospheric models. In this technique, no averaging or smoothing of the opacities is employed; rather, the opacities are accurately computed at a few frequencies scattered over the entire spectrum. Tests have shown that 500–600 frequency points are sufficient for an accuracy in the final model of better than 50 K. In our calculations we use 1010 frequencies. The opacity of H_2O is treated as a straight mean.

A problem of some concern is the fact that, while all the model atmospheres were computed under the standard approximation of plane-parallel geometry, Betelgeuse is a supergiant star with a very large atmosphere, and one must be concerned about the possible effects of sphericity. In the plane-parallel approximation, the assumption is made that the extent of the atmosphere is small compared to the radius of the star. A simple test can therefore be made of this assumption numerically. A model representative of α Ori ($T_{\rm eff} = 3800$ K, log $g = 0$) has an atmospheric extent (between $\tau = 1$ and $\tau = 10^{-4}$) of 1.2×10^7 km. Based on the radius for the star ($R = 650\ R_\odot$, see § II*b*), the ratio of atmospheric height to radius is 0.03, and this alone would lead us to believe that the plane-parallel approximation will not introduce significant errors in our models. A more rigorous test has been provided by the study of the sphericity effects of late-type stars by Watanabe and Kodaira (1978, 1979). They have constructed spherical, nongray static LTE model atmospheres in five different sets to investigate the effects of sphericity. Briefly, they find that sphericity leads to an increase in atmospheric extent, almost no difference in color, a slight decrease in absolute visual magnitude, and strengthening in such temperature-sensitive molecular bands as TiO and H_2O due to the cooling resulting from the divergence of the radiative flux in the outer layers of the spherical atmosphere. In some cases, especially for such extended atmospheres as in long-period variables, the effects are predicted to be quite spectacular. However, we note that model B1 of Watanabe and Kodaira, which has parameters quite representative of those of Betelgeuse, has a value of $\eta = 3\%$, where η is their parameter measuring atmospheric extent, and such a small value produces very small changes in atmospheric structure. Finally, the molecular lines, which have been chosen in our study, are formed fairly deep in the atmosphere; consequently they are not expected to be greatly influenced by the cooling which would result from our taking into account the effects of sphericity. All these considerations appear to indicate that no significant errors are being introduced by our use of model atmospheres based on plane-parallel geometry.

b) The Defining Parameters

i) *The Effective Temperature*

The flux distribution of the continuous spectrum is set by the stellar atmosphere (the temperature distribution, surface gravity, the chemical composition, etc.), and the interstellar and circumstellar reddening. Several methods have been proposed for extracting $T_{\rm eff}$ from the continuous spectrum. In the infrared, outside the major molecular bands, the absorption-line density is quite low so that a measurement of the continuum flux is possible via photometry. The intrinsic infrared monochromatic flux provides a relation between the surface area (proportional to the square of the angular diameter) and the emergent infrared flux per unit area (a quantity which depends—approximately linearly—on the effective temperature and which is computed using a model atmosphere). The total integrated flux emitted by the star provides a second relation between the surface area and the effective temperature ($T_{\rm eff}^4$ in this case). Thus, the combination of the observed infrared and total fluxes with an estimate of the reddening provides the angular diameter and $T_{\rm eff}$—see, for example, Blackwell, Petford, and Shallis (1980). Augason *et al.* (1979; also Augason 1980) report new spectrophotometry which they combine with flux distributions predicted by model atmospheres (Tsuji 1976*a*; Faÿ and Johnson 1973) to obtain $T_{\rm eff}$: $T_{\rm eff} = 3850$ K if $A_v = 0.8$ mag and $T_{\rm eff} = 3740$ K if $A_v = 0.3$ mag—see Appendix A for a discussion of the extinction (A_v). The uncertainty apart from that contributed by A_v is ± 50 K. The $T_{\rm eff}$ as obtained from the infrared flux method does not change with phase.

Tsuji (1976*b*) collated published infrared spectrophotometry and multicolor photometry. A comparison between the composite energy distribution and the predictions of his line blanketed atmospheres led Tsuji to conclude that $T_{\rm eff} = 3900$

± 150 K. Analysis of their photometry (1.3–2.2 μm) led Kodaira *et al.* (1979) to propose $T_{\rm eff} = 3800 \pm 100$ K.

An alternative method for deriving $T_{\rm eff}$ from the continuous spectrum uses the single relation between the total integrated flux and the angular diameter. Tsuji (1976*b*, 1978, 1979) argues that this method is too consistent with an effective temperature of about 3800 K rather than the lower values (e.g., $T_{\rm eff} = 3250$ K—Dyck, Lockwood, and Capps 1974) sometimes associated with it. An independent analysis of published angular diameter measurements leads White (1980) to propose $T_{\rm eff} = 3680$ K. He suggests that the published angular diameter measurements hint at a ± 8 milli-arcsec variation ($\pm 18\%$ change in angular diameter) over the 5.8 year period. Since the total flux does not vary more than a few percent (Dyck, Lockwood, and Capps 1974; Augason 1980), the angular diameter variation implies that $T_{\rm eff}$ must vary by ± 300 K, but, as White notes, this is larger than the range (± 60 K) indicated by the narrow-band photometric measurements of the spectral type.

The atoms and molecules in the stellar atmosphere are also potential thermometers. The necessary observations for atomic lines will be difficult to collect because molecular lines obliterate large portions of the spectrum. In principle, a vibration-rotation band from a bound electronic state should be an excellent thermometer (Hinkle and Lambert 1975). We considered the CO and OH bands as potential thermometers; NH provides an insufficient number of lines.

Although the OH $\Delta v = 1$ V-R bands are well represented, the rotational and vibrational temperatures are not obtainable. Examination of the OH line list shows that there is a moderately tight correlation between equivalent width (W_σ) and the excitation potential of the lower level ($\chi_{\rm exc}$). The maximum width of the W_σ versus $\chi_{\rm exc}$ plot is just 0.8 eV for a narrow W_σ range and ~ 0.4 eV over most of the plot. Since the majority of the OH lines are off the weak-line portion of the curve of growth, the adopted effective temperature (hence, rotation temperature) fixes the shape of the curve but not the scatter of the points about a mean curve. If the microturbulence, which also fixes the shape of the curve, were known accurately, the effective temperature might be obtainable. The key to the problem is to observe the weak low-excitation OH lines which are largely in a spectrum interval obliterated by the Earth's atmosphere. The $\Delta v = 2$ OH lines provide a similar distribution in a W_σ versus $\chi_{\rm exc}$ plot. In addition, CO, CN, and the neutral atoms crowd the 1.6 μm window and limit the number of measureable weak OH lines.

The CO $\Delta v = 3$ bands near 1.6 μm provide the best opportunity to determine the excitation or rotation-vibration temperature. The range in $\chi_{\rm exc}$ is about 2 eV at all W_0 levels. The CO 1.6 μm lines confirm that $T_{\rm eff} \approx 3800$ K because the C abundances provided by the individual lines and our adopted model atmosphere show no trend with excitation potential. We estimate the uncertainty to be ± 250 K. The uncertainty could probably be reduced by a detailed consideration of line blending and/or a thorough spectrum synthesis of selected regions containing high- and low-excitation lines. The derived $T_{\rm eff}$ depends slightly on the adopted surface gravity: $\Delta T_{\rm eff} = \pm 50$ K for $\Delta \log g = \pm 0.5$. This result is quite consistent with the $T_{\rm eff}$ estimates based upon the continuous spectrum.

We adopt $T_{\rm eff} = 3800 \pm 100$ K. This estimate is consistent with most of the above results. We assign high weight to the result provided by Augason *et al.* (1980). This $T_{\rm eff}$ overlaps the temperature of a M2 III star for which Tsuji (1981) with the infrared flux method obtains $T_{\rm eff} = 3800 \pm 40$ K. The referee suggests that because spectral classifications are based on TiO band strengths, supergiants should be at least 100 K cooler than a giant of the same type. Then, if the spectral type of α Ori at the time of our observations was M2.8 (see § III), the $T_{\rm eff}$ according to Tsuji's $T_{\rm eff}$ scale for M giants should be $T_{\rm eff} = 3570$ K, not 3800 K. Although this lower temperature appears to be excluded by the infrared flux method, we shall discuss how the derived abundances are changed when $T_{\rm eff}$ is decreased from 3800 K to 3600 K.

ii) *The Surface Gravity*

The surface gravity may be calculated from estimates of the stellar radius and mass. A standard expression relates the radius, $T_{\rm eff}$ and the bolometric magnitude $M_{\rm bol}$. Wilson (1976) gives the absolute visual magnitude $M_v = -5.9$ from a Ca II K line width and the revised Hyades distance modulus. A confirming M_v estimate is derived from Wilson's (1959)'s observation that α Ori and HD 14270, a supergiant in the h and χ Persei cluster, have equal K line widths, and Humphreys (1978)'s measurement of the cluster distance modulus ($M_v = -5.8$ for HD 14270). For α Ori, we adopt $M_v = -5.85$ and a bolometric correction BC $= -1.55$ (Lee 1970) to obtain $M_{\rm bol} = -7.4$ and, then $R/R_\odot = 620$ for $T_{\rm eff} = 3800$ K.

A second estimate of the radius is provided from the observed angular diameter and distance estimates. By combining the mean apparent magntitude $m_v = 0.8$, $A_v = 0.7$, and $M_v = -5.85$, we obtain a distance $d = 155$ pc. After a discussion of available angular diameter measurements, White (1980) recommends a mean angular diameter (total limb-darkening assumed and an empirical correction for the effect of circumstellar dust) of $\phi = 0\farcs043$. This is close to the result ($\phi = 0\farcs041$ for $A_v = 0.7$) derived by Augason *et al.* (1979) by the infrared flux method. We adopt $\phi = 0\farcs041$ to obtain a radius $R/R_\odot = 680$. We shall adopt a straight average of our two estimates: $R/R_\odot = 650$.[3]

When $M_{\rm bol}$ and $T_{\rm eff}$ are known, the stellar mass is, in principle, obtainable by an inspection of a theoretical H-R diagram. Unfortunately, the evolutionary tracks of massive stars like α Ori are most sensitive to the input physics of a stellar evolution calculation. Evolutionary tracks computed by Lamb, Iben, and Howard (1976) suggest $M \approx 15\ M_\odot$ for α Ori. Other tracks computed with higher opacities and apparently other differences (Stothers and Chin 1977; see also Stothers and Chin 1979) give $M \approx 30\ M_\odot$. Cloutman and Whitaker (1980) adopt a new theory of convection and evolve a $15\ M_\odot$ model toward the red giant branch. On the new theory, the red supergiant is brighter by about 0.14 dex in $\log L/L_\odot$. This luminosity increase corresponds to a mass increase from 15 $M_\odot$ to about 21 $M_\odot$ according to tracks given by Lamb *et al.* Additional factors comprising the identification of the mass via the H-R diagram include the composition and mass loss before the red giant branch. We adopt a probable range $10 < M/M_\odot < 30$ or $-0.2 < \log g < 0.3$ for $R/R_\odot = 650$.

The requirement that neutral and ionized lines of an element yield the same abundance is commonly used to determine the surface gravity of a late-type star. We adopted a variant of this method. We selected some unblended weak and moderately strong lines of neutral atoms (Na I, Si I, Ti I, Fe I, Ni I) from Reticon spectra with $\lambda \gtrsim 10000$ Å (see Table 1). This region is

[3] White estimates M_v from the measured narrow-band CN index (Wing 1971; White and Wing 1978) and a CN-index versus M_v relation. He obtains $=96$ pc and a mean radius $R/R_\odot = 460$ for $\phi = 0\farcs043$.

TABLE 1

THE ATOMIC LINE LIST

Species	λ (Å)	χ (eV)	W_λ (mÅ)	log *gf*
Na I	10746.45	3.19	79	−1.48
Si I	10301.44	6.10	22	−1.97
	10694.25	5.96	142	−0.41
Ti I	10066.55	2.16	191	−1.79
Cr I	9900.95	2.99	173	−1.93
Fe I	10007.32	3.02	91	−4.72
	9889.05	5.03	198	−0.30
	10265.23	2.22	199	−4.57
Ni I	10193.25	4.05	186	−0.73

not marred by TiO lines, and intervals exist where CN lines are also unimportant contributors. The spectra had been taken for a variety of different projects but were well suited to our purpose. We obtained *gf*-values from solar equivalent widths and the Holweger-Müller (1974) model solar atmosphere. Abundances were obtained for a grid of α Ori models.

The microturbulent velocity is set by the requirement that the weak and strong lines of Si I and Fe I provide the same abundance. The result depends only slightly on the model atmosphere: the $T_{\rm eff} = 3800$ K and $\log g = 0$ model gives $\xi = 3$ km s^{-1}. The Na, Si, and Fe abundances were obtained from the weakest lines. In a plot of the abundance against $T_{\rm eff}$ (for a fixed log *g*), the Si (and Fe) and Na loci have a quite different slope and their intersection gives a $T_{\rm eff}$, log *g* solution. Our assumption that Si, Fe, and Na have the same relative abundances in the sun and α Ori allows us to combine the low (Na) and high (Si, Fe) ionization potential species as a surface gravity monitor (for a given effective temperature).

Unless the atmosphere is now severely depleted in H and enriched in He, we expect the metal abundance to fall between the solar value and the slightly higher value exhibited by the younger Hyades cluster (Branch, Lambert, and Tomkin 1980) and the yellow Ib supergiants (Luck 1977, 1979); i.e., [Fe/H] ~ 0.0–0.2, where $[X] = \log X_\alpha - \log X_\odot$.

The Na, Si and Fe loci show a very close approach for $T_{\rm eff} = 3800$ K and [Fe/H] ≈ 0.2 at $\log g \approx -1$. These estimates are temperature dependent; the former estimate becomes $\log g \sim 0$ for $T_{\rm eff} = 3900$ K. We see that these metallic lines provide rough confirmation of our earlier estimate of the surface gravity. Our adoption of LTE is a probable source of systematic error. The weak 6 eV Si I line is formed deep in the atmosphere, and, hence, LTE may be a reasonable assumption. Na may be overionized relative to LTE (Auman and Woodrow 1975), and, hence, the present estimate of the surface gravity for a fixed $T_{\rm eff}$ may be an underestimate. With this latter qualification, we find that the metallic lines just confirm the surface gravity derived from mass and radius estimates. We adopt a surface gravity $\log g = 0.0 \pm 0.3$.

III. OBSERVATIONS

High-resolution infrared spectra of α Ori are our primary source of lines. The several spectra (see Table 2), which collectively provide almost complete coverage of the atmospheric windows from 1.4 to 5.3 μm, were acquired at the KPNO 4 m reflector with the new Fourier transform spectrometer (Hall *et al.* 1978). The resolution was $\Delta\sigma > 0.07$ cm^{-1} after apodization. The signal-to-noise ratio (S/N) exceeded 100 over almost the entire spectrum. Some spectra were corrected for the telluric absorption lines by ratioing the α Ori spectrum to the nearly continuous spectrum of the embedded carbon star IRC +10216 or the planet Mercury.

TABLE 2

INFRARED SPECTRA

Wavenumber Region	Date	Resolution[a]	S/N[a]
2390–2800	1977 Oct 21	0.060	250
2830–3100	1980 Feb 5	0.070	230
4000–5100, 5550–6600	1980 Feb 5	0.070	130
4000–5100, 5550–6600	1980 Aug 26	0.036	280

[a] 1977 Oct 21 unapodized, observed with prototype FTS. Other spectra apodized with Norton and Beer 1976 function I2.

Long stretches of the infrared spectrum are crowded with absorption lines. The idea that the infrared is a source of unblended lines is largely a myth for cool stars like α Ori. Fortunately, myth and fact are synonymous for the 3–4 μm spectra, after ratioing to a reference star to remove the telluric lines the spectrum contains few stellar lines. This region contributes the important OH and NH V-R lines. Figure 1 illustrates the cleanness of the 3–4 μm spectra.

Selected intervals in the red and near-infrared were observed at the McDonald Observatory using the Reticon-equipped coudé spectrometer at the 2.7 m reflector (Vogt, Tull, and Kelton 1978). Resolutions of 0.1–0.2 Å were used. When telluric lines were a severe contaminant, a hot star was observed at a similar air mass.

α Ori is a semiregular variable with a period of 5.8 years. The molecular lines do not vary by large amounts. The equivalent widths of CO $\Delta v = 2$ lines near 1.6 μm and the CN 2 μm lines vary by less than about 10%–15% on the several spectra spanning a number of years; the earlier spectra were obtained at the McDonald Observatory with the JPL Fourier transform spectrometer (Beer, Norton, and Seaman 1971). The weaker OH $\Delta v = 1$ lines for which coverage is less complete also show no significant change from spectrum to spectrum. The CN red system near 8000 Å has also been observed at the McDonald Observatory; equivalent width changes are again slight. We assume that observations from different epochs may be combined and analyzed with a model atmosphere for a mean set of atmospheric parameters. Our line selection is weighted in favor of lines obtained from the 1980 February spectra when α Ori was near minimum light (spectral type M2.8 Ib according to White 1980) so that the photosphere might have been cooler than normal.

Our analysis is based on equivalent width measurements. For NH, OH, and CN lines, all available lines were inspected and only the lines with a well-defined profile were included in the final line lists. Very few of the CO 1.6 μm lines are cleanly resolved from neighboring lines. In this window, we measured a selection of well-resolved lines of all species to calibrate the equivalent width versus central depth relation. Then, the central depth of CO lines was measured and their equivalent width computed from the calibration. This use of partly blended lines provided a larger sample of lines than would have been achieved with a strict adherence to the criteria employed in the selection of the NH, OH, and CN lines. The selected lines of a set appear, as expected, to yield very nearly identical abundance. The standard deviations of the abundances are determined partly by equivalent width errors (location of continuum, undetected blends, and measurement uncertainties due to noise) and by (small) systematic errors in the *f*-values. The standard deviations are ±0.14 (CO, 48 lines),

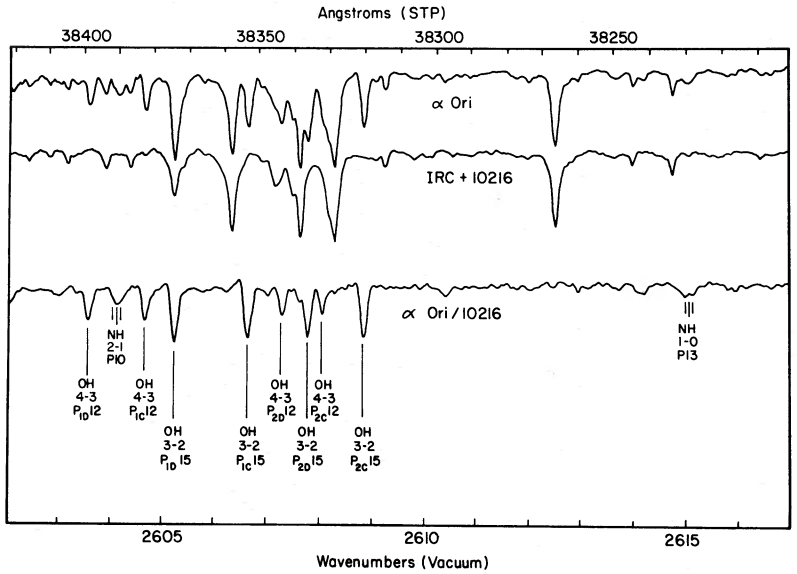

FIG. 1.—The Betelgeuse spectrum from 2602 to 2617 cm^{-1} showing two NH triplets and two OH quartets. Note the greater width of the NH lines. The upper spectrum is the observed spectrum showing several telluric lines. The middle spectrum is IRC +10216, which is featureless in this region and has been used to divide out the telluric features. The lower spectrum is the stellar spectrum with telluric lines removed.

± 0.10 (NH, 13 lines), ± 0.05 (OH, 62 lines) and ± 0.11 (CN, 10 lines). The mean error attributable to equivalent width uncertainties is small relative to other sources of uncertainty and systematic error (see below).

IV. THE ABUNDANCE ANALYSIS

a) CO *and* OH

Our abundance analysis uses the weak overtone ($\Delta v = 3$) $^{12}C^{16}O$ lines in the 5600–6700 cm^{-1} atmospheric window. Table 3 lists lines with $\log W_\sigma/\sigma < -5.1$ but stronger lines were also examined. The stronger first-overtone ($\Delta v = 2$) $^{12}C^{16}O$ lines offer a check on the $\Delta v = 3$ lines but are primarily monitors of the velocity field and the structure of the upper photosphere. The fundamental ($\Delta v = 1$) CO lines are very strong; the line cores, which provide little abundance information, offer a test of the thermal structure of the upper photosphere. We postpone a discussion of the $\Delta v = 1$ lines. We do not discuss the lines of the $^{13}C^{16}O$ and other isotopically substituted molecules.

The OH radical is detectable through the vibration-rotation transitions of the $X\ ^2\Pi$ ground state. The fundamental vibration-rotation transitions were discovered in the Betelgeuse spectrum by Beer *et al.* (1972). The new spectra provide equivalent widths of fundamental ($\Delta v = 1$, 3–4 μm) OH lines. A composite curve of growth is shown in Figure 2. We comment in the Appendix on our selection of the first-overtone OH lines (see Table 4). The theoretical curve of growth in Figure 2 is computed for a microturbulence of $\xi = 3$ km s^{-1}. The CO lines suggest a slightly higher value. Our

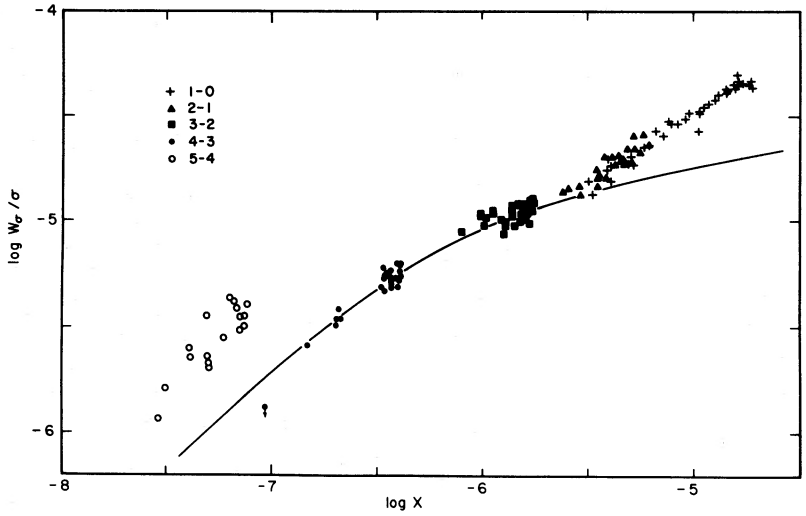

FIG. 2.—A composite curve of growth for OH fundamental lines. The abscissa is $\log X = \log gf - \theta(W_\sigma)\chi$. $\theta(W_\sigma)$ is the excitation temperature. Note that the 5–4 lines are displaced from the theoretical curve of growth fitted to the 4–3 and 3–2 lines. The solid curve is a theoretical curve of growth for a line of lower state potential $\chi = 1.14$ eV and frequency $\sigma = 2935$ cm^{-1}, for the case where the microturbulence is a constant 3 km s^{-1} throughout the atmosphere.

TABLE 3

CO SECOND-OVERTONE VIBRATION-ROTATION LINES

Band	Line	σ (cm^{-1})	W_σ (cm^{-1})	log gf	χ'' (eV)
3–0.....	*P*51	6023.7	0.028	−7.78	0.627
	*P*49	6041.4	0.041	−7.79	0.579
	*P*47	6058.7	0.040	−7.80	0.534
	*P*5	6330.2	0.046	−8.59	0.007
	*R*60	6380.9	0.040	−7.13	0.862
	*R*69	6350.3	0.038	−7.02	1.134
4–1.....	*P*74	5715.4	0.015	−7.05	1.553
	*P*65	5811.8	0.023	−7.08	1.265
	*P*61	5852.1	0.028	−7.10	1.148
	*P*58	5881.4	0.037	−7.11	1.065
	*P*1	6267.4	0.020	−8.64	0.266
5–2.....	*P*73	5650.0	0.017	−6.62	1.770
	*P*56	5823.3	0.034	−6.69	1.267
	*R*76	6156.3	0.045	−5.90	1.872
	*R*79	6141.4	0.032	−5.87	1.977
	*R*81	6130.8	0.026	−5.85	2.049
6–3.....	*P*56	5746.5	0.037	−6.36	1.520
	*R*0	6117.0	0.024	−7.89	0.787
	*R*77	6069.9	0.031	−5.58	2.153
	*R*84	6032.3	0.028	−5.50	2.404
	*R*88	6008.3	0.014	−5.45	2.557
7–4.....	*P*56	5669.8	0.024	−6.08	1.769
	*P*4	6019.3	0.034	−7.04	1.048
	*R*96	5872.4	0.010	−5.11	3.117
8–5.....	*P*37	5751.9	0.040	−5.98	1.614
	*R*63	5966.4	0.045	−5.27	2.201
	*R*70	5939.7	0.032	−5.18	2.408
	*R*78	5902.3	0.015	−5.09	2.669
	*R*79	5897.1	0.018	−5.08	2.704
	*R*89	5838.6	0.010	−4.97	3.070
9–6.....	*P*25	5756.2	0.041	−5.90	1.691
	*P*16	5807.5	0.045	−6.06	1.607
	*P*13	5822.8	0.044	−6.14	1.586
	*P*12	5827.6	0.043	−6.17	1.581
	*P*2	5870.8	0.022	−6.91	1.547
	*R*9	5908.7	0.036	−6.16	1.566
	*R*63	5886.0	0.031	−5.08	2.442
	*R*84	5788.2	0.008	−4.84	3.116
10–7.....	*P*14	5740.3	0.024	−5.94	1.838
	*R*9	5830.4	0.028	−5.98	1.812
	*R*55	5830.0	0.027	−5.01	2.472
11–8.....	*R*7	5747.2	0.023	−5.93	2.047
	*R*11	5757.0	0.030	−5.74	2.064
	*R*13	5761.3	0.030	−5.66	2.075
	*R*24	5777.1	0.036	−5.36	2.167
	*R*37	5778.8	0.034	−5.11	2.344
	*R*39	5777.5	0.028	−5.08	2.377
	*R*49	5763.9	0.031	−4.94	2.571
	*R*52	5757.6	0.032	−4.90	2.638

abundance analysis is based on $\xi = 4$ km s^{-1}; note that with this value the theoretical curve will also fit the weaker 2–1 OH lines. Since our line selection includes weak lines, the abundances are insensitive to the microturbulence with a change $\Delta\xi = 2$ km s^{-1} leading to $\Delta \log \epsilon(\mathrm{X}) \sim 0.04$. Macroturbulence must be included when fitting line profiles.

The CO lines provide the C abundance almost independently of an assumption about the O abundance. The near independence from the O abundance occurs because C is fully associated into CO throughout the greater part of the atmosphere. The partial pressure of O is set by the abundance difference (O − C) and, therefore, analysis of the OH lines provides not the O abundance but a locus in the O versus C abundance plane along which the (O − C) abundance difference is nearly constant. The intersection of this locus with the corresponding locus from the CO line analysis defines the C and O abundances. We derived the CO and OH loci for a grid of atmospheres centered on the adopted atmospheric parameters for α Ori. The abundances corresponding to the adopted parameters ($T_{\rm eff} = 3800$ K and log = 0.0) are

$$\log \epsilon(\mathrm{C}) = 8.41 \text{ and } \log \epsilon(\mathrm{O}) = 8.77\ ,$$

where we adopt $^{12}\mathrm{C}/^{13}\mathrm{C} = 6$ to present the total ($^{12}\mathrm{C} + {}^{13}\mathrm{C}$) abundance. The uncertainties attributable to $T_{\rm eff}$ and log g uncertainties are summarized later.

The [O I] lines are useful abundance indicators for G and K giants and supergiants. With the intent of extending their role to M stars, we obtained Reticon echelle spectra of the [O I] lines at 6300 and 6363 Å. To our dismay, the C and O abundances provided by the CO and OH lines did not predict the observed W_λ's of the [O I] lines. The predictions for the 6300 Å line ($W_\lambda \approx 200$ mÅ) far exceed the observations ($W_\lambda \approx 45$ mÅ).

Inspection of a spectrophotometric scan (Faÿ, Stein, and Warren 1973) shows that the TiO γ' system $\Delta v = 0$ sequence depresses the 6300–6363 Å region. We obtained a series of overlapping Reticon exposures over the interval 6100–6500 Å with a single exposure covering 100 Å at a resolution of 0.2 Å. The B2 III star γ Ori was also observed. On the composite spectrum showing the flux ratio α Ori/γ Ori, we interpolated the continuum between the interval 6100–6160 Å beyond the red-degraded γ' 0–0 head and the region around 6500 Å. This continuum clearly shows that the local continuum adopted in the measurement of the [O I] lines off echelle spectra is severely depressed below the interpolated continuum (Fig. 3).

The γ' system line lists are incomplete. The 0–0 band contribution near 6300 Å comes from high rotational lines (Phillips 1973). Laboratory observations of the 1–1 band (Hocking, Gerry, and Merer 1979) do not extend to 6300 Å. We expect this and the 2–2 band to contribute to the continuum depression. We estimate that there are between 10 and 20 TiO lines

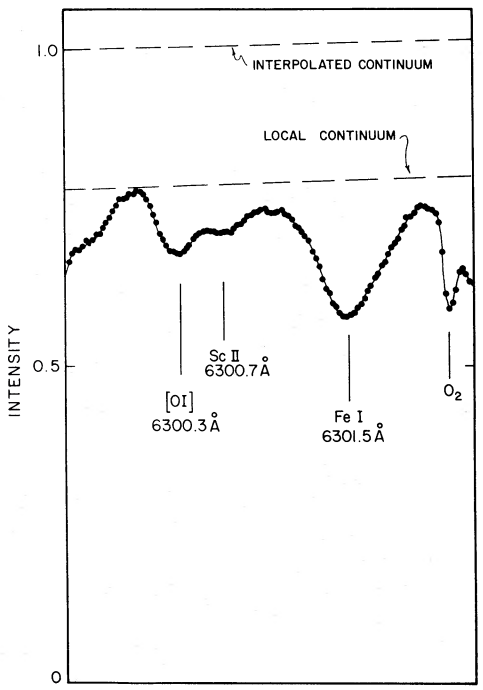

FIG. 3.—A portion of an echelle spectrum around the [O I] 6300.3 Å line. The local continuum is set from the interval ±10 Å about the [O I] line. The interpolated continuum is defined using the 6100–6500 Å interval.

TABLE 4

OH FUNDAMENTAL VIBRATION-ROTATION LINES

Band	Line	σ (cm^{-1})	W_σ (cm^{-1})	log gf[a]	χ'' (eV)
1–0.....	P_1 + 8.5	3235.6	0.150	−4.42	0.164
	9.5	3188.5	0.140	−4.34	0.205
	10.5	3142.1	0.140	−4.27	0.250
	11.5	3092.6	0.140	−4.21	0.299
	12.5	3044.4	0.131	−4.20	0.353
	15.5	2890.0	0.102	−4.00	0.539
	16.5	2839.0	0.094	−3.95	0.609
	19.5	2675.9	0.062	−3.83	0.841
	20.5	2672.9	0.054	−3.80	0.926
	21.5	2565.5	0.051	−3.77	1.014
	22.5	2511.5	0.042	−3.74	1.105
	P_1 − 9.5	3189.4	0.150	−4.34	0.205
	12.5	3043.2	0.137	−4.15	0.353
	13.5	2994.3	0.123	−4.09	0.411
	14.5	2941.9	0.112	−4.04	0.473
	16.5	2837.4	0.077	−3.95	0.609
	17.5	2785.9	0.082	−3.91	0.682
	18.5	2730.3	0.070	−3.87	0.760
	20.5	2620.9	0.049	−3.80	0.926
	21.5	2567.5	0.047	−3.77	1.014
	22.5	2509.6	0.045	−3.74	1.105
	P_2 + 8.5	3193.7	0.160	−4.39	0.210
	9.5	3143.2	0.140	−4.32	0.255
	11.5	3047.5	0.130	−4.18	0.357
	13.5	2945.6	0.108	−4.07	0.477
	14.5	2892.4	0.097	−4.02	0.542
	16.5	2786.1	0.082	−3.93	0.685
	17.5	2733.5	0.074	−3.89	0.763
	19.5	2624.0	0.050	−3.82	0.928
	20.5	2566.6	0.040	−3.79	1.017
	21.5	2512.6	0.039	−3.75	1.108
	P_2 − 8.5	3194.3	0.150	−4.39	0.210
	9.5	3145.5	0.140	−4.32	0.255
	11.5	3046.6	0.132	−4.18	0.357
	12.5	2996.9	0.121	−4.13	0.415
	13.5	2944.5	0.122	−4.07	0.477
	14.5	2893.5	0.095	−4.02	0.542
	15.5	2839.6	0.087	−3.98	0.612
	16.5	2787.5	0.084	−3.93	0.685
	18.5	2679.0	0.061	−3.85	0.844
	19.5	2622.5	0.050	−3.82	0.928
	20.5	2568.6	0.045	−3.79	1.017
	21.5	2510.9	0.034	−3.75	1.108
2–1.....	P_1 + 10.5	2991.3	0.078	−4.09	0.683
	12.5	2896.7	0.081	−3.96	0.782
	13.5	2846.8	0.074	−3.90	0.838
	14.5	2798.7	0.056	−3.85	0.897
	15.5	2747.0	0.057	−3.80	0.960
	16.5	2697.6	0.055	−3.75	1.028
	17.5	2644.2	0.047	−3.71	1.098
	19.5	2539.1	0.037	−3.63	1.251
	P_1 − 9.5	3037.0	0.090	−4.16	0.639
	10.5	2990.3	0.070	−4.09	0.683
	14.5	2797.3	0.054	−3.85	0.897
	15.5	2748.5	0.053	−3.80	0.960
	16.5	2696.0	0.060	−3.76	1.028
	17.5	2645.9	0.044	−3.71	1.098
	18.5	2592.0	0.038	−3.70	1.173
	P_2 + 8.5	3041.5	0.080	−4.21	0.645
	9.5	2995.5	0.077	−4.13	0.688
	10.5	2947.4	0.063	−4.06	0.735
	11.5	2899.9	0.074	−4.00	0.786
	12.5	2849.9	0.074	−3.93	0.842
	13.5	2801.1	0.056	−3.88	0.901
	14.5	2749.5	0.056	−3.83	0.964
	15.5	2699.5	0.044	−3.78	1.031
	16.5	2646.4	0.043	−3.72	1.102
	17.5	2595.2	0.035	−3.70	1.176
	P_2 − 11.5	2899.0	0.066	−4.00	0.786
	12.5	2850.9	0.064	−3.93	0.842
	13.5	2800.1	0.053	−3.88	0.901
	14.5	2750.6	0.052	−3.83	0.964
	15.5	2698.3	0.044	−3.78	1.031
	16.5	2647.6	0.039	−3.72	1.102
	18.5	2542.2	0.035	−3.66	1.254
3–2.....	P_1 + 8.5	2929.5	0.040	−4.22	1.016
	9.5	2885.4	0.036	−4.13	1.054
	11.5	2795.6	0.036	−3.98	1.141
	12.5	2750.4	0.031	−3.92	1.191
	13.5	2702.0	0.027	−3.86	1.244
	14.5	2655.3	0.032	−3.81	1.301
	15.5	2605.1	0.028	−3.76	1.362
	16.5	2557.1	0.026	−3.71	1.426
	17.5	2505.3	0.024	−3.69	1.494
	P_1 − 4.5	3089.8	0.027	−4.71	0.905
	6.5	2971.6	0.039	−4.32	0.982
	9.5	2886.3	0.033	−4.13	1.054
	11.5	2796.6	0.035	−3.98	1.141
	12.5	2749.3	0.033	−3.92	1.191
	13.5	2703.3	0.030	−3.86	1.244
	14.5	2654.0	0.029	−3.81	1.301
	15.5	2606.5	0.028	−3.75	1.362
	16.5	2555.6	0.022	−3.71	1.426
	P_2 + 9.5	2864.3	0.034	−4.11	1.100
	10.5	2799.7	0.029	−4.02	1.146
	11.5	2753.7	0.033	−3.96	1.195
	12.5	2705.2	0.027	−3.86	1.248
	13.5	2657.8	0.026	−3.84	1.305
	14.5	2607.7	0.026	−3.78	1.366
	15.5	2559.0	0.028	−3.74	1.430
	16.5	2507.4	0.027	−3.69	1.498
	P_2 − 5.5	3021.3	0.032	−4.50	0.960
	7.5	2935.2	0.035	−4.28	1.022
	9.5	2845.7	0.036	−4.11	1.100
	11.5	2752.9	0.030	−3.96	1.195
	12.5	2706.1	0.033	−3.89	1.248
	13.5	2656.8	0.030	−3.84	1.305
	14.5	2608.8	0.025	−3.78	1.366
	15.5	2557.9	0.029	−3.74	1.430
	16.5	2508.6	0.027	−3.69	1.498
4–3.....	P_1 + 2.5	3001.8	<0.004	−5.09	1.275
	4.5	2933.1	<0.004	−4.84	1.305
	5.5	2895.9	0.009	−4.67	1.326
	8.5	2778.1	0.017	−4.30	1.412
	9.5	2735.4	0.017	−4.21	1.478
	10.5	2693.3	0.017	−4.12	1.488
	11.5	2648.4	0.015	−4.05	1.532
	12.5	2604.5	0.015	−3.98	1.579
	13.5	2557.6	0.014	−3.91	1.630
	14.5	2512.2	0.015	−3.86	1.685
	P_1 − 4.5	2932.8	0.008	−4.84	1.305
	5.5	2896.4	0.010	−4.67	1.326
	9.5	2736.2	0.015	−4.21	1.478
	10.5	2692.4	0.014	−4.12	1.488
	11.5	2649.4	0.016	−4.05	1.532
	12.5	2603.5	0.017	−3.98	1.579
	13.5	2558.8	0.012	−3.91	1.630
	P_2 + 5.5	2867.4	0.011	−4.61	1.358
	8.5	2741.1	0.014	−4.26	1.453
	10.5	2652.6	0.014	−4.09	1.536
	11.5	2607.9	0.013	−4.01	1.584
	12.5	2560.9	0.014	−3.95	1.634
	13.5	2514.8	0.012	−3.89	1.689
	P_2 − 5.5	2867.2	0.010	−4.61	1.358
	9.5	2697.3	0.016	−4.17	1.493
	10.5	2653.3	0.013	−4.09	1.536
	11.5	2607.1	0.013	−4.01	1.584
5–4.....	P_1 + 5.5	2740.3	0.003	−4.74	1.705
	7.5	2665.2	0.009	−4.63	1.756
	8.5	2626.4	0.008	−4.59	1.787
	9.5	2585.2	0.011	−4.40	1.822
	10.5	2544.4	0.009	−4.30	1.861
	P_1 − 5.5	2740.7	0.008	−4.74	1.707
	7.5	2665.8	0.006	−4.63	1.756
	10.5	2543.5	0.008	−4.30	1.861
	11.5	2501.8	0.010	−4.21	1.902
	P_2 + 5.5	2713.2	0.004	−4.86	1.736
	6.5	2673.2	0.006	−4.71	1.763
	7.5	2632.9	0.006	−4.57	1.793
	8.5	2590.9	0.008	−4.36	1.827
	P_2 − 5.5	2713.0	<0.003	−4.86	1.736
	6.5	2673.5	0.007	−4.70	1.763
	7.5	2632.5	0.005	−4.57	1.793
	8.5	2591.4	0.009	−4.36	1.827
	9.5	2548.5	0.011	−4.35	1.865
	10.5	2505.8	0.010	−4.26	1.907

[a] The gf-values are computed from Mies's 1974 A-values. See the text for the values used in the abundance analysis.

TABLE 5

NH FUNDAMENTAL VIBRATION-ROTATION LINES

BAND	LINE	σ (cm^{-1})	W_σ (cm^{-1})	LOG gf			χ'' (eV)
				P_1	P_2	P_3	
1–0.....	*P*3	3023.8	0.025	1.06-5	9.20-6	4.97-6	0.024
	5	2950.1	0.030	1.38-5	1.21-5	9.06-6	0.061
	9	2789.9	0.029	1.57-5	1.44-5	1.25-5	0.181
	10	2747.4	0.025	1.54-5	1.42-5	1.26-5	0.221
	12	2659.9	0.017	1.45-5	1.35-5	1.23-5	0.311
	13	2614.9	0.017	1.40-5	1.31-5	1.20-5	0.362
	15	2522.7	0.007	1.29-5	1.22-5	1.13-5	0.474
2–1.....	*P*6	2763.0	0.023	4.11-5	3.66-5	2.91-5	0.469
	7	2724.8	0.019	4.32-5	3.89-5	3.22-5	0.496
	8	2685.5	0.022	4.44-5	4.04-5	3.45-5	0.527
	9	2645.2	0.018	4.53-5	4.15-5	3.61-5	0.561
	10	2604.0	0.018	4.57-5	4.21-5	3.73-5	0.599
	12	2519.1	0.013	4.57-5	4.27-5	3.87-5	0.686

Å^{-1} near 6300 Å. At this density, TiO provides a quasi-continuous opacity. This explains why the [O I] lines appear anomalously weak on the echelle spectra in which the expected atomic lines appear without obvious perturbation by intruding TiO lines.

The realization that the TiO molecule sets the local continuum level across large stretches (perhaps, all) of the visible and near-infrared spectrum removes a useful abundance indicator from our original set of atomic and molecular lines. This fact must be faced in analyses of *all* absorption lines in this region. Eventually, it should be possible to include, at least in a statistical approximation, the overlying TiO lines in the opacity calculations and to complete an abundance analysis; Luck and Lambert (1982) discuss such an analysis of the Li I 6707 Å doublet.

b) NH *and* CN

The NH lines provide one estimate of the N abundance. Several lines (unresolved triplets) of the 1–0 and 2–1 V-R bands were first identified by Lambert and Beer (1972). We have identified additional lines on a KPNO spectrum—see Table 5 and Figures 1 and 4. The $\Delta v = -3$ bands of the CN red system cross the window providing the NH and OH lines. Fortunately, these CN lines are predicted and observed to be very weak; we estimate that the CN contribution to an NH line does not exceed about 10%. The partial pressure of free N is set by N_2 molecule formation with the result that the NH density scales approximately as $\epsilon(\mathrm{N})^{1/2}$. The N abundance for $T_{\rm eff} = 3800$ K, $\log g = 0.0$, and $\xi = 4$ km s^{-1} is

$$\log \epsilon(\mathrm{N}) = 8.62 .$$

In this temperature range, an NH line's intensity is insensitive to the adopted surface gravity but moderately sensitive to the effective temperature.

The CN lines in spectra of G and K giants often assume the role of the N abundance indicator. In this analysis, the CN lines may play a supporting role thanks to the presence of the NH V-R lines. The demotion of CN is welcomed because the CN density is controlled by the C, N, *and* O abundances and plagued by the uncertain dissociation energy. With the adopted model and the O abundance provided by the CO and OH lines, the CN lines (Table 6) provide a locus in the $\log \epsilon(\mathrm{N})$–$\log \epsilon(\mathrm{C})$ plane—see Figure 5. If CN is considered to be a C abundance monitor, the abundance provided by the CN-NH intersection is 0.25 dex less than that provided by the CO lines.

If the several sources of error peculiar to CN are assessed, this difference of 0.25 dex is just acceptable. We note that the locus shifts with the adopted O abundance such that $\Delta \log \epsilon(\mathrm{O}) \approx \Delta \log \epsilon(\mathrm{C})$. For a fixed chemical composition, the CN lines in contrast to CO, NH, and OH lines weaken with decreasing temperature. Therefore, atmospheric inhomogeneities (see below) are likely to introduce systematic errors in

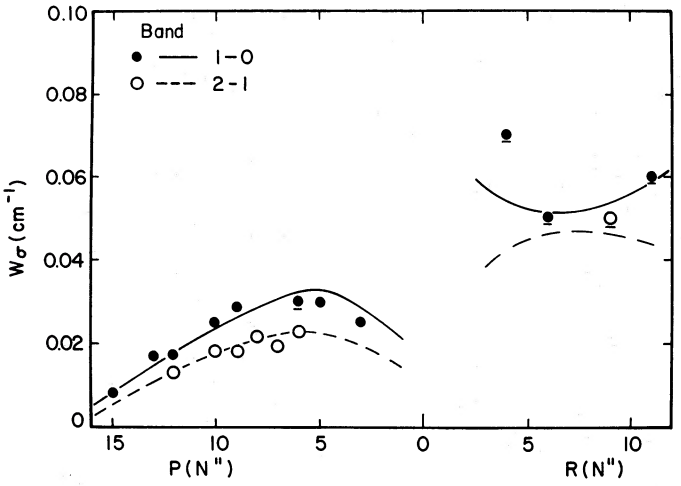

FIG. 4.—NH vibration-rotation lines in the Betelgeuse spectrum. The underlined symbols denote the uncertain measurements. The predicted variations of the equivalent width in the *P*- and *R*-branches is shown.

TABLE 6

2 MICRON CN RED SYSTEM LINES

Band	Line	σ (cm^{-1})	W_σ (cm^{-1})	log gf	χ'' (eV)
0–2.....	$P_1 44$	4609.6	0.024	−2.16	0.956
	$Q_1 48$	4703.8	0.036	−1.79	1.040
	$Q_2 58$	4555.0	0.028	−1.72	1.281
	$R_1 29$	5022.1	0.035	−2.27	0.702
1–3.....	$P_2 30$	4623.7	0.027	−2.06	0.961
	$P_2 32$	4598.0	0.028	−2.03	0.990
	$Q_2 44$	4567.1	0.036	−1.56	1.198
	$Q_2 45$	4553.8	0.037	−1.55	1.218
2–4.....	$Q_1 30$	4508.9	0.032	−1.63	1.203
	$Q_2 32$	4504.4	0.029	−1.62	1.231

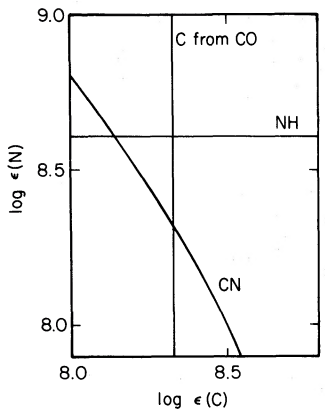

FIG. 5.—Abundance solutions for NH and CN for the adopted model together with the C abundance derived from CO lines.

our analysis between CN and the other three molecules. Note further that our line list is composed largely of measurements of the 1980 Feburary spectra when α Ori was at minimum light. On the other hand, our adopted dissociation energy, $D_0{}^0 = 7.52$ eV, is at the low end of the range suggested by recent measurements. The CN locus in Figure 5 is translated along the log ϵ(C) axis by $\Delta \log \epsilon(\mathrm{C}) \approx -1.4\,\Delta D_0{}^0(\mathrm{eV})$; if $D_0{}^0 = 7.9$ eV were adopted, a value suggested by a recent shocktube experiment (see Appendix B) and several earlier experiments, the C abundance would be 0.8 dex less than that provided by the CO lines. If the solar CN lines with independently determined C and N abundances are used to establish the CN oscillator strengths for a given $D_0{}^0$ analyzing the C abundance derived from the CN lines in α Ori is within about 0.2 dex of that from CO for all reasonable $D_0{}^0$ values.

As the sole electronic transition in the analysis, the CN lines may be subject to NLTE effects (Hinkle and Lambert 1975). However, our test calculations based on the simplifying assumption that the atmosphere is not severely optically thick to lines of the CN red system show that errors incurred by our use of LTE should not amount to more than a 0.1 dex translation of the CN locus in Figure 5. In short, the CN lines are presently consistent with the abundances provided by the CO, NH, and OH lines, but a reexamination of the issue will be called for if future experiments put the dissociation energy higher than $D_0{}^0 = 7.65$ eV.

c) *The Atmosphere*

Three principal factors determine the accuracy of the final abundances: (i) the basic molecular data, (ii) the quality of the spectra, and (iii) the model atmosphere. In this section, we discuss this third factor. In addition to summarizing the consequences of incorrect choices for the defining parameters ($T_{\rm eff}$ and log g), we comment on possible inconsistencies and deficiencies in the assumptions behind the construction of the model atmosphere.

The effects of alternative choices of effective temperature and surface gravity on the abundances are summarized in Figure 6. Note that the selections of lines and basic molecular data used in the construction of this figure differ slightly from the final choices so that Figure 6 does not provide the abundances quoted earlier for the standard model, but such differences are immaterial when Figure 6 is used to obtain the temperature and gravity dependences of the abundances. Our estimates $\Delta T_{\rm eff} = \pm 100$ K and $\Delta \log g = \pm 0.3$ correspond to $\Delta \log \epsilon = \pm 0.15$ dex or less. Abundance ratios are less sensitive to the defining parameters, e.g., the N/O ratio changes by less than 0.05 dex over the same range of $\Delta T_{\rm eff}$ and $\Delta \log g$. At $T_{\rm eff} = 3600$ K, an alternative considered at the referee's request, the C abundance is reduced by 0.12 dex, the N (from NH) and the O abundances by 0.25 dex. The consistency of the abundance information from CN and the other molecules is marginally improved for $T_{\rm eff} = 3600$ K. The difference in the C abundances from CO and CN (see Fig. 5) of 0.20 dex at $T_{\rm eff} = 3800$ K is cut to 0.12 dex at $T_{\rm eff} = 3600$ K. With the selected OH oscillator strengths, oxygen is underabundant relative to the sun by 0.4 dex if $T_{\rm eff} = 3600$ K and log $g = 0.0$. Stellar evolutionary calculations (see § V) predict much smaller reductions of the surface oxygen abundance. Then, a selection of $T_{\rm eff} = 3600$ K would require that either these calculations lack an essential ingredient causing ON-cycled material to contaminate the surface or the adopted OH oscillator strengths are too large by a factor of 3. Although a recent experiment (Podolske and Johnston 1983) is consistent with the latter suggestion, current ab initio calculations of demonstrably high accuracy would preclude this simple explanation—see Appendix B. In short, the oxygen abundance tends to confirm selection of $T_{\rm eff} = 3800$ K rather than a temperature of 3600 K or below.

Since the atmospheric structure is influenced by the atomic and molecular line blanketing, it is, in principle, necessary to iterate on the abundances in order to achieve agreement between the adopted and derived abundances. Tsuji's (1979) discussion of such an iteration shows that the corrections are small for the abundance differences reported here. His first set of abundances differed from the assumed values by −1.17, +0.88, and −0.01 for C, N, and O, respectively. At the conclusion of the iterative procedure, the final abundances differed from the first (and inconsistent) set by just −0.03, −0.05, and 0.10 dex for C, N, and O, respectively. Our final results are consistent at the ±0.05 dex level with the input abundances of the model. Turbulent pressure is an additional source of uncertainty. A majority of our calculations used models not including the turbulent pressure. Models at $T_{\rm eff} = 3800$ K and log $g = 0.0$ with and without the turbulent pressure ($\xi_{\rm mic} = 3$ km s^{-1}) give abundances from CO, OH, and NH differing by only 0.02 (C), 0.00 (N), and 0.03 (O) dex.

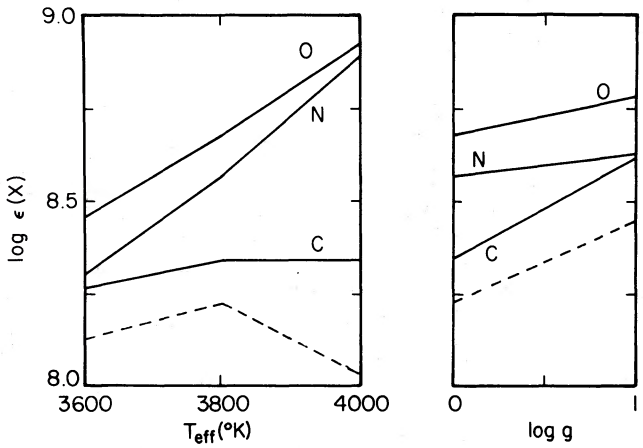

FIG. 6.—The C, N, and O abundances as a function of $T_{\rm eff}$ and log g. The solid lines show the results from CO, NH, and OH. The broken lines show the C abundance derived from CN lines and the O and N abundances provided by the other molecules.

Our analysis is based on weak lines whose region of formation overlaps that of the continuum. Tsuji (1979) shows that a model atmosphere quite similar to ours predicts satisfactorily the observed flux distribution from the visible to the infrared. This provides a partial check on the model atmosphere. In addition, the predicted relation between color temperature on the Wing system and effective temperature from the models and the empirical relation (Ridgway *et al.* 1980) agree very well (Piccirillo, Bernat, and Johnson 1981).

Evidence that the formation of the stronger lines is not fully understood surfaced when we examined the stronger CO and OH lines—see, for example, Figure 2 showing a composite curve of growth for OH lines. Possible causes for the failure of the model to predict the observed curve of growth include: a steep gradient of the microturbulence in the upper photosphere (more generally, a velocity field with relative flows of at least 1–3 km s^{-1}); a steeper temperature gradient in the upper photosphere; the presence of supergranules (Schwarzschild 1975); departures from LTE and/or plane-parallelism of the atmosphere (see § II for a discussion of atmospheric sphericity).[4] The upper photospheric temperatures can probably not be reduced sufficiently to increase the equivalent widths to the observed value. The central intensity of the cores of the strongest CO lines at 2.3 and 5.0 μm set a limit on the boundary temperature.

Schwarzschild suggested that the surface of a cool supergiant might be composed of a small number of large granules. Clearly, different properties of the emergent spectrum will exhibit a different weighting across the granule distribution (and with time, if the number of granules is very small). On the 1980 February 5 spectrum, the strong $\Delta v = 1$ OH absorption lines are accompanied by weak emission in the high-frequency (blue) wing; the emission has an equivalent width about 10% that of the absorption component. This emission is clear evidence that the real atmosphere is more complex than our models; e.g., granulation or a warm expanding chromosphere is present. It is unlikely that the weak lines employed in our abundance analysis are seriously affected by this departure from the predicted atmospheric structure. Additional observations to monitor the OH (and other) profiles would be of interest.

Direct evidence for surface inhomogeneities was provided by Goldberg *et al.* (1982) from speckle interferometry through a 20 Å bandpass at 6500 Å. Their preliminary report discusses a single observation in which they found a bright spot contributing about 0.08 mag to the integrated brightness. Growth and decay of active regions and their rotation across the disk are suggested by the observations of changes in the linear polarization at visible wavelengths (Hayes 1980).

The vibrational (and rotational) levels of the electronic ground states should be close to LTE (Thompson 1973; Hinkle and Lambert 1975). A definitive calculation of the departures from LTE in the V-R transitions of CO and OH cannot yet be provided because the data on the collision cross sections are incomplete. In particular, additional theoretical and/or experimental results are needed for vibrational excitation by H atoms. The fact that the OH and CO curves of growth are similar may be evidence that NLTE is not at the root of the problem.

If the microturbulence increases to 10 km s^{-1} at the top of the photosphere, the fit of the predicted equivalent widths to the observed ones is improved. The increase in turbulence could be viewed as the heating mechanism underlying the chromosphere.

Our selection of CO, NH, and OH lines as the primary abundance indicators should minimize the systematic errors arising from our inadequate modeling of the atmosphere and line formation. This asertion is made on three grounds: (i) weak lines are used for the abundance analysis, (ii) the (LTE) variation of the molecular abundances with temperature and pressure changes are moderately similar for these three molecules, and (iii) the CN molecule with a different temperature sensitivity generally confirms the results of the CO, NH, and OH analysis.

V. DISCUSSION

The CO, NH, and OH lines with the adopted model ($T_{\rm eff}$ = 3800 K, log g = 0.0, ξ = 4 km s^{-1}) provide the abundances log ϵ(C) = 8.41, log ϵ(N) = 8.62, and log ϵ(O) = 8.77. The abundances relative to the sun (Lambert 1978) are [C] = −0.26, [N] = +0.63 and [O] = −0.15. If, as expected, α Ori is metal rich, the differences [X] abundance relative to the star's initial composition must be decreased by the metal enhancement [Fe/H] where [Fe/H] $\approx$ +0.1 is likely. The abundance uncertainties arising from uncertainties in $T_{\rm eff}$, log g, and ξ, and equivalent width uncertainties are about $\pm$0.15 dex. Systematic and ill-defined uncertainties are contributed by our inadequate representation of the atmosphere and deficiencies in the molecular data. Corrections to the abundances arising from adjustments to the three-model atmosphere parameters are of the same sign for the three elements. Hence, the abundance ratios C/N/O are less affected by such changes. Our results give [C/O] = −0.18 and [N/C] = +0.96. Since the CNO cycles, a probable source of the composition changes, conserve CNO nuclei, it is of interest to compare the total (including ^{13}C) CNO abundance: we find [CNO] = −0.04 relative to the sun; i.e., when the abundance uncertainties are recognized, it appears that the CNO nuclei have been conserved.

In summary, the composition of Betelgeuse's atmosphere is currently log ϵ(C) = 8.4, log ϵ(N) = 8.6, and log ϵ(O) = 8.8. The C/N ratio is distinctly nonsolar, [N/C] = +0.9. This strong N enrichment together with the conservation of the total C, N, and O abundance points to the contamination of the atmosphere with CN-processed material. The slight O deficiency, [O] = −0.15, may reflect the operation of the slower ON-cycles (or even higher temperature nuclear processing) but may also have a more mundane explanation—the difference from the solar abundance is not really significant in the light of the abundance uncertainties.

Comment is surely required on the fact that we did not confirm the several earlier reports of a large C deficiency in the atmosphere. Brief explanatory comments on inadequacies of certain earlier analyses were given in § I. Here, we refer to the papers by Tsuji (1979) and Jura and Morris (1981). Tsuji's (1979) model atmosphere analysis considered CO, OH, and CN lines. Equivalent widths of CO 2–0 and OH $\Delta v = 1$ lines were taken from the literature: Spinrad *et al.* (1970) for CO and Beer *et al.* (1972) for OH. Photographic 8 Å mm^{-1} plates provided the CN equivalent widths. A model atmosphere

[4] The empirical curve of growth is suggestive of a large damping constant. Although the curve may be reproduced by a theoretical curve, the required collisional damping constant is a factor of about 1000 larger than expected for OH molecules in the low pressure atmosphere of Betelgeuse. A quick check also shows that neither the existence of hyperfine splitting nor satellite components will account for the empirical curve of growth.

analysis with $T_{\rm eff} = 3900 \pm 150$ K and $\log g = 0.0$ led to a C underabundance by a factor of 20, i.e., a factor of 10 below our result. The N and O abundances are within 0.2 dex of our values. The discrepancy is, in large part, due to the high microturbulence assumed by Tsuji ($\xi = 9$ km s^{-1}) in analyzing the lines of CO, OH, and CN. None of the lines are on the weak-line portion of our curves of growth. Dr. Tsuji very kindly analyzed one of our CO lines with his $T_{\rm eff} = 3800$ K, $\log g = 0.0$, and $\xi = 3$ km s^{-1} model to obtain a C abundance within 0.1 dex of our result. This agreement shows that the model atmosphere and spectrum analysis programs are not the origin of the discrepant C abundances.

Jura and Morris (1981) derive the photospheric C/H ratio from observations of the circumstellar CO radio emission and the K I 7699 Å fluorescent emission. Carbon was reported to be deficient by a factor of 25. New observations of the surface brightness of the circumstellar K I emission led Mauron *et al.* (1984) to a higher C abundance and a deficiency of 6 and a factor of 3 less than our photospheric abundance. Jura and Morris noting our earlier and preliminary report of a near-solar C abundance (Lambert 1974) did identify two possible sources of error in their analysis: the expanding shell is far from spherically symmetric and/or the C atoms in the shell are not associated into CO molecules. These and other factors now deserve scrutiny.

The high N and ^{13}C abundances point to the presence of CN-cycle processed material in the atmosphere. The deep convective envelope of a red giant or supergiant is predicted to dredge up processed material (see Lamb, Iben, and Howard 1976 for discussion of a 15 $M_\odot$ supergiant). A second dredge-up is predicted for intermediate mass stars on their return to the red giant branch following He core exhaustion. Kaler, Iben, and Becker (1978) put the upper mass limit for a second dredge-up at 8–10 $M_\odot$ and, therefore, α Ori is unlikely to (have) suffer(ed) the small incremental change in CNO abundances resulting from the second dredge-up. For the first dredge-up, Becker and Iben (1979) predict $[^{12}C] = -0.19$, $[^{14}N] = +0.53$, and $[^{16}O] = -0.04$ for a 11 $M_\odot$ star (see their Table 6D), the most massive star considered by them. If their predictions for 7, 9, and 11 $M_\odot$ stars are extrapolated to a star of mass 15 $M_\odot$, one obtains $[^{12}C] \approx -0.22$, $[^{14}N] \approx +0.69$, and $[^{16}O] \approx -0.10$. The observed values are $[^{12}C] = -0.43$, $[^{14}N] = +0.53$, and $[^{16}O] = -0.25$ if α Ori is assumed to be slightly metal rich relative to the Sun [Fe/H] = +0.1. As discussed above, the influence of the model atmosphere on the abundances is reduced when abundance ratios are considered. The observed changes are $[^{12}C/^{14}N] = -0.96$, $[^{14}N/^{16}O] = +0.78$, and $[^{12}C/^{16}O] = -0.08$ if α Ori began with the solar ratios of C, N, and O. These results compare favorably with the predictions: $[^{12}C/^{14}N] = -0.81$ to -0.96, $[^{14}N/^{16}O] = +0.56$ to $+0.79$, and $[^{12}C/^{16}O] = -0.15$ to -0.12, where the second entry for each quantity refers to the extrapolated results for a 15 $M_\odot$ star. These observed and predicted ratios are in good agreement considering the remaining uncertainties. The $^{12}C/^{13}C$ ratio points to a deficiency in the calculations. The observed $^{12}C/^{13}C$ ratio (6) is below the predicted $^{12}C/^{13}C$ (~ 20) values. The origin of the excess ^{13}C relative to the prediction is uncertain, but the additional processing of ^{12}C to ^{13}C and ^{13}C to ^{14}N can be accomplished without a major perturbation of the predicted C/N/O abundance ratio. We note that Cloutman and Whitaker (1980) propose that existing calculations underestimate the size of the convective core. A larger core and a smaller envelope should result in lower C/N and $^{12}C/^{13}C$ ratios after the dredge-up on the red giant branch. Unfortunately, they did not follow their calculations through to the dredge-up. Mass loss prior to the development of the convective envelope will also produce C/N and lower $^{12}C/^{13}C$ ratios—see Harris and Lambert (1984) who discuss the $^{16}O/^{17}O/^{18}O$ ratios.

Before a complete understanding of α Ori's surface composition is reached, additional work is essential. We conclude by identifying several key tasks. The CNO analysis could be made more precise. This will require: (i) accurate measurements of the V-R transition probabilities for OH and NH; (ii) an accurate determination of the band f-values of the CN red system lines and the CN dissociation energy; (iii) a thorough study of the strong molecular lines in order to glean information about the atmospheric structure; (iv) reobservation and analysis at several different phases to eliminate errors incurred by combining spectra obtained at different times. Careful studies of the CNO abundances in OB stars are needed in order to eliminate the possibility that unexpected CNO abundances in a red supergiant are simply the result of the standard evolution of a star with a nonstandard initial composition. Finally, a sample of red supergiants should be analyzed in order to determine the range in the CNO abundances. A considerable number of these tasks may be tackled and solved with currently available means.

We thank Drs. T. Tsuji, G. C. Augason, and W. J. Stevens for helpful correspondence, Dr. B. Gustafsson for a critical review of a draft of the paper, Dr. R. H. Tipping for providing a listing of the CO f-values, Dr. M. Larsson for extensive and lively discussions on the f-values for the CN red system, and Mr. D. B. Slavsky for computing line strengths for the OH and NH V-R transitions. We also thank Drs. J. Tomkin and P. L. Cottrell for assistance at the telescope, and Dr. J. F. Dominy for his enthusiastic assistance with the calculations. We thank the anonymous referee for constructive comments and, in particular, for the suggestion that we consider a lower effective temperature. A part of the paper was written while D. L. L. was on sabbatical leave. He thanks Professor P. Erman and Dr. B. Gustafsson for their hospitality. At the University of Texas, this research has been supported in part by the National Science Foundation (grants AST 79-22014, 79-13109, 81-17485, and 82-05800) and the Robert A. Welch Foundation of Houston, Texas.

APPENDIX A

INTERSTELLAR AND CIRCUMSTELLAR EXTINCTION

The total extinction for α Ori is often set near $A_v \approx 0.7$ mag; for example, Tsuji (1976*b*) adopted $A_v = 0.68$ mag. Two $(B-V)$ measurements and assumed intrinsic colors gave $E_{B-V} = 0.22$ mag (Johnston 1967) and 0.18 mag (Lee 1970) which with a third (uncertain) estimate of $E_{B-V} = 0.16$ mag (Eggen 1973) provided a mean $E_{B-V} = 0.19$ mag and $A_v/E_{B-V} = 3.6$ (Lee 1970) gave $A_v = 0.68$ mag.

Intrinsic colors of M supergiants were checked by Johnson

and Mendoza (1966) who obtained the same E_{B-V} from samples of early-type stars and M supergiants in the h and χ Persei cluster, and then remarked that this observation was a valid check on the M stars' intrinsic colors because neither stellar sample had been used to establish the adopted intrinsic colors. Observations of the southern M supergiant HD 90586 also offer a check on these colors. White and Wing's (1978) measurements of a TiO index show that this supergiant is within a subclass of α Ori. HD 90586 has a nearby blue companion with $E_{B-V} = 0.45$ mag (Humphreys, Strecker, and Ney 1972). On the assumption that the pair form a physical system, we deduce that $E_{B-V} = 0.26$ mag for α Ori, an estimate slightly larger than Tsuji's adopted value.

White (1980) reported $A_v = 0.71$ mag for α Ori from observations of a reddening-independent TiO index and a near-infrared color. Observations of bright M giants, which are assumed to be unreddened, provide the TiO index-intrinsic color calibration. White assumes that this calibration is applicable to M supergiants. However, TiO bands are predicted to be weaker in supergiants unless the microturbulence is larger than in giants (Johnson, Mould, and Bernat 1982; Johnson and Steinman-Cameron 1982). A rough estimate is $A_v \approx 0.5$ mag pending a direct calibration of the TiO index in supergiants. Note that this estimate includes the nongray contribution of circumstellar grains, whereas standard A_v estimates derived from a color index include a circumstellar contribution only to the extent that dust shell around α Ori differs from the typical shell of the sample used to derive the intrinsic color.

Betelgeuse is near the "Orion Northwest" region where $A_v \approx 0.2$–0.3 mag (Lee 1970). A limit $A_v < 0.3$ mag seems appropriate because α Ori is probably less distant than the Orion stars. However, interstellar extinction is patchy. The circumstellar contribution to A_v is probably small. Since the excess infrared emission represents a small fraction of the total stellar luminosity, the extinction introduced by the circumstellar grains is small unless the grain albedo is remarkably high. Mass loss over an extended period may have driven grains far away from the star. Such cold grains, which would not emit strongly at 11 μm, could supplement the extinction provided by the interstellar grains.

In summary, the extinction for α Ori is not yet well determined, but the range 0.3 mag $< A_v <$ 0.8 mag is likely to encompass the true value.

APPENDIX B

BASIC DATA FOR MOLECULAR LINES

a) Carbon Monoxide

The vibration-rotation transitions within the $^1\Sigma^+$ ground state of CO are prominent features of the infrared spectrum of a cool star. Our abundance analysis uses the $^{12}C^{16}O$ $\Delta v = 3$ lines in the 5600–6700 cm^{-1} atmospheric window.

Precise frequencies for many vibration-rotation lines have been measured. We computed the frequencies for additional lines from molecular constants. We adopt oscillator strengths provided by Chackerian and Tipping (1983). Their calculations employ a dipole moment function which is derived from measurements of the line (or band) absorption coefficients for the leading bands of the sequences; e.g., 1–0, 2–0, 3–0, and 4–0. These new results do not differ substantially from an earlier recipe (Tipping 1976). The mean difference over the sample of $\Delta v = 3$ $^{12}C^{16}O$ lines is less than 0.1 dex. The oscillator strengths should be accurate ($\pm 10\%$) for at least the leading bands in the $\Delta v = 3$ sequence or $\pm 20\%$ for the lines employed in the abundance analysis. A systematic error could be expected to increase with increasing vibrational and rotational energy as the transition matrix element depends more heavily on the dipole moment function at internuclear separations outside the range covered adequately by the laboratory measurements of cool or cold CO gas.

We have compared the oscillator strengths with theoretical calculations by Kirby-Docken and Liu (1978). The theoretical results for the $\Delta v = 2$ sequence are about 10% to 15% smaller for the stellar lines in our list. The difference is larger for the $\Delta v = 3$ sequence lines. The theoretical results are about 40% smaller for low rotational lines in the *P*- and *R*-branches. The difference increases to about 70% for high members of the *P*-branch and decreases to near 20% for the *R*-branch. The appearance of these differences for the low-excitation lines, which have been the subject of several laboratory experiments, suggests that the theoretical results are not as accurate as the adopted oscillator strengths.

b) The Imidyl Radical

The V-R transitions within the $^3\Sigma^-$ state of NH have been ignored until recently by laboratory spectroscopists. Frequency predictions were discussed by Lambert and Beer. Bernath and Amano (1982) have since provided accurate frequencies for lines of the 1–0 band from *P*(4) to *R*(5). An ab initio calculation of the $X\,^3\Sigma^-$ state was reported by Das, Wahl, and Stevens (1974; see also Stevens 1973) who predicted the band oscillator strengths for the V-R transitions. Their method of Optimized Valence Configurations, which is discussed in detail by Wahl and Das (1970), was also applied to OH (see below).

Inspection of Figure 5 shows that the *R*-branch triplets are markedly stronger than their *P*-branch counterparts. Our suspicion that the vibration-rotation interaction was responsible for this effect was confirmed by a calculation. We combined the dipole moment function provided by Das, Wahl, and Stevens with the RKR-potential energy curve for the $X\,^3\Sigma^-$ state to obtain the *gf*-values given in Table 5. The predicted and observed variation of W_σ along the *P*- and *R*-branches are compared in Figure 5; the splitting of the components comprising a triplet was taken into account in the predictions. The accuracy of the *gf*-values is likely to be comparable to the similar predictions for OH for which we estimate an uncertainty of $\pm 25\%$. It is seen that the strongest lines in the *R*-branch are approximately twice as strong as the *P*-branch members. The greater part of this difference originates with the V-R interaction. The change in the triplet splitting along the *R*-branch is largely responsible for the unusual variation of W_σ with N''.

The NH dissociation energy is set at $D_0^0 = 3.46 \pm 0.03$ eV (Graham and Lew 1978; Zetzsch 1978).

c) *The Hydroxyl Radical*

The OH radical is detectable through the vibration-rotation transitions of the $X\ ^2\Pi$ ground state. Accurate line positions for $\Delta v = 1$ and 2 lines are provided by Maillard, Chauville, and Mantz (1976) and Beer (1975). The dissociation energy of OH is well determined from spectroscopy: $D_0^0 = 4.391 \pm 0.002$ eV (Carlone and Dalby 1969).

Oscillator strengths for the OH lines were originally taken from Mies (1974) who made a detailed calculation of OH transition probabilities by combining a theoretically derived electric dipole moment function and a composite RKR-theoretical molecular potential. The theoretical calculation (Stevens *et al.* 1974) predicts to a satisfying precision a variety of the experimentally determined properties of the OH ground state; for example: the dissociation energy $D_e = 4.53$ eV fits the observed value $D_e = 4.63$, and the computed dipole moment for the ground state $\mu = 1.680$ *D* is close to the experimental value $\mu = 1.660 \pm 0.010$ *D*. The reader is referred to Stevens *et al.* (1974) for a discussion of their ab initio method of Optimized Valence Configurations (OVC) and a detailed comparison of the predicted and observed OH properties.

Although their comparison encourages confidence in the OH oscillator strengths, a direct confrontation between the theoretical and experimental oscillator strengths would be of interest. Available measurements of absolute oscillator strengths (see Mies for references; also Roux, d'Incan, and Cerny 1973) are not of sufficient accuracy to provide the necessary test. Fortunately, Mies noted that relative oscillator strengths provide an excellent test of the dipole moment function. Relative oscillator strengths for fundamental and first-overtone lines and the strong vibration-rotation interaction in several bands have been measured. Mies (1974, pp. 170–171) shows how the available measurements confirm the shape and scale of the dipole moment function. His calculations should provide reliable absolute oscillator strengths.

We attempt an assessment of the oscillator strengths by performing our own calculations with two dipole moment functions: the Stevens *et al.* function and a second ab initio (configuration interaction or CI) calculation (Chu, Yoshimine, and Liu 1974). A comparison of the predicted and observed molecular properties suggests that the optimized valence configuration calculation is slightly superior. Our calculations are based upon an RKR potential and numerical evaluation of the transition matrix elements. Although we do not include the spin-uncoupling, the results are indicative of the effect of a change in the dipole moment function. We find that the CI dipole moment function predicts lower oscillator strengths for the *P*-branch fundamental lines which comprise the Betelgeuse line list: the ratio $f(\text{OVC})/f(\text{CI})$ for a representative stellar line is approximately 1.6, 1.8, 2.0, and 2.3 for the bands 1–0, 2–1, 3–2, and 4–3, respectively. The sense of the ratio is quite consistent with the different slopes of the dipole moment functions near the equilibrium internuclear separation. A similar comparison for the first-overtone bands gives $f(\text{OVC})/f(\text{CI}) \approx 1.3$, 1.3, 1.4, and 1.5 for the 2–0, 3–1, 4–2, and 5–3 bands, respectively. The ratio of the oscillator strengths for first-overtone to fundamental transitions offers a test of a theoretical dipole moment function; for example, Murphy (1971) measured a transition probability ratio $a = A(2, 0)/A(2, 1) = 0.44 \pm 0.03$ for initial members of the *Q*-branch. Mies notes that his calculations reproduced this ratio or $a = 0.46 \pm 0.06$. We find that the CI dipole moment function gives a value of a which is substantially larger. The ratio $b = A(3, 1)/A(3, 0)$ with a mean experimental ratio $b = 1.15 \pm 0.05$ is not quite so well matched by Mies's calculations; his average is $b = 1.62$ with a range of 1.34–2.44. We find that the CI dipole moment function gives $b = 7.4$–2.6 for low P lines. On the basis of these tests, the OVC calculation appears to be superior. The ratio $f(\text{OVC})/f(\text{CI})$ surely indicates the maximum error.

As our abundance analysis was being completed, Werner, Rosmus, and Reinsch (1983) published calculations based on MCSCF-SCEP wave functions. Their calculations provide lower rotationless Einstein *A*-values than Mies predicted from the OVC results: $f(\text{OVC})/f(\text{SCEP}) = 1.5$, 1.4, 1.3, and 1.1 for the bands 1–0, 2–1, 3–2, and 4–3, respectively. Werner *et al.* noted that their predicted *A*-values agreed to within about 10% with estimates by Argawalla, Manocha, and Setser (1981) who measured the infrared emission from OH radicals produced by reactions with known rate constants ($H + NO_2$ and $H + ClO_2$). Analysis of solar pure rotation transitions from the $v'' = 0$, 1, and 2 levels also suggests that Werner *et al.*'s electric dipole moment function is superior to the OVC prediction used by Mies (Sauval *et al.* 1984). Our final abundance analysis is based on a combination of Mies's results for the 4–3 band normalized to the rotationless *A*-value listed by Werner *et al.* This compromise is not expected to result in a significant error. The adopted oscillator strengths are probably accurate to $\pm 25\%$.

A discordant note must be acknowledged. Podolske and Johnston (1983) using a tunable diode laser to sense OH measured an integrated absorption coefficient of $S = (3.3 \pm 1.5) \times 10^{-20}$ cm^2 mol^{-1} cm^{-1} for the P_1–(4.5) transition. This compares with $S = 1.06 \times 10^{-19}$ cm^2 mol^{-1} cm^{-1} from Mies's calculations (see Gillis and Goldman 1981) and $S \approx 7.1 \times 10^{-20}$ cm^2 mol^{-1} cm^{-1} from Werner, Rosmus, and Reinsch (1983). The factor of 2 discrepancy between experiment and the MCSCF-SCEP prediction would seem to fall outside the range permitted by the ab initio calculations.

Our analysis of the stellar equivalent widths for the $\Delta v = 1$ sequence confirmed one limitation of Mies's theoretical *f*-values. A curve of growth (Fig. 2) shows the lines from the 5–4 band displaced by about 0.5 dex from the smooth curve defined by the lines from the bands 1–0 through to 4–3. Mies notes (see his Fig. 2 and accompanying text) that the transition probabilities for the 5–4 and the adjacent 4–3 and 6–5 bands were sensitive to the precise shape of the dipole moment function. The astronomer more familiar with atomic spectroscopy may note that this sensitivity arises from the molecular (vibrational) analog of severe cancelation of the radial integral involving atomic wave functions. A search for the 6–5 band was unsuccessful; the upper limits on the equivalent width do not allow us to determine if the band falls on the extension of the smooth curve from the 1–0 to 4–3 bands. The 4–3 band (and other bands to a lesser extent) may also be affected by the cancelation. The 4–3 band is important because it provides many of the weak lines which yield an abundance almost independently of assumptions about the microturbulence. Since the 4–3 and 3–2 bands define a curve close to the shape of the predicted curve of growth, the 4–3 *f*-values are probably not seriously in error. The 5–4 band is not included in the abundance analysis. It appears unlikely that use of Werner *et al.*'s *f*-values will place all OH lines on the predicted curve of growth.

The *f*-values of the $\Delta v = 2$ lines are not so sensitive to the dipole moment function, and, therefore, these lines would appear to be superior abundance indicators to the $\Delta v = 1$ lines. Unfortunately, our search did not locate OH lines on the weak line portion of the curve of growth. The high line density in the 1.6 μm window is one responsible factor. In addition, many of the weak OH lines fall in regions of low atmospheric transmission. The weakest OH lines provide an O abundance (at a fixed C abundance) consistent with the result provided by the $\Delta v = 1$ lines.

d) The CN *Radical*

The CN red system ($A\ ^2\Pi$–$X\ ^2\Sigma^+$) is an electronic transition providing observable lines from the red to the near-infrared. Initially, we selected lines from the $\Delta v = +2$ sequence around 8000 Å but rejected them when we realized that TiO provides a weak blanket of unresolvable lines. The $\Delta v = -2$ sequence near 2 μm dominates the absorption lines there. Our selection (Table 6) of lines from the 0–2, 1–3, and 2–4 bands is but a small representative sample of the available lines.

A direct and accurate measurement of the band *f*-values for the $\Delta v = -2$ sequence is unavailable—see Sneden and Lambert (1982) who summarize the available experimental results. Fortunately, accurate *f*-values are provided by an ab initio calculation (Larsson, Siegbahn, and Ågren 1983). These predictions are similar to but more accurate than those published by Cartwright and Hay (1982—see also Sneden and Lambert 1982). Larsson *et al.* note that their calculations reproduce the limited available experimental results on the red system and the relative $f_{v'v''}$-values derived by Sneden and Lambert (1982) from the solar spectrum. In short, we expect the adopted *f*-values to be accurate to about $\pm 15\%$.

The dissociation energy D_0^0(CN) is a continuing source of uncertainty for abundance analyses drawing on CN lines. Larsson *et al.* predict $D_0^0 = 7.52$ eV from their CN calculations and a scaling factor obtained from their predicted and the measured dissociation energy of N_2. The D_0^0 uncertainty is impossible to quantify; Larsson *et al.* write "one can probably safely state that $7.4 < D_0^0(\mathrm{CN}) < 7.7$ eV." Solar CN lines may also be used to estimate D_0^0; for example, the 0–0 lines with f_{00} from Larsson *et al.* and the C and N abundances from either CH *A*–*X* and NH *A*–*X* lines or OH *A*–*X* and the permitted N I lines give $D_0^0 = 7.51 \pm 0.05$ eV almost independently of the choice of a model solar atmosphere; this derivation is based on results provided by Lambert (1978). The close agreement between this estimate and Larsson *et al.*'s prediction is surely fortuitous. A recent and, perhaps, the most reliable of the experimental measurements is $D_0^0 = 7.65 \pm 0.05$ eV (Engleman and Rouse 1975). Confusion and contradiction continue with a shocktube experiment (Colket 1984) providing $D_0^0 = 7.93 \pm 0.07$ eV and an oscillator strength for the violet system in fine agreement with the accurate result obtained from radiative lifetime measurements. We adopt $D_0^0 = 7.52$ eV but consider the consequences of a higher D_0^0.

REFERENCES

Argawalla, B. S., Manocha, A. S., and Setser, D. W. 1981, *J. Phys. Chem.*, **85**, 2873.
Augason, G. C. 1980, private communication.
Augason, G. C., Taylor, B. J., Erickson, E. F., and Witteborn, F. C. 1979, *Bull. AAS*, **11**, 645.
Auman, J. R. 1969, *Ap. J.*, **157**, 799.
Auman, J. R., and Woodrow, J. E. J. 1975, *Ap. J.*, **197**, 163.
Becker, S. A., and Iben, I., Jr. 1979, *Ap. J.*, **232**, 831.
Beer, R. B. 1975, private communication.
Beer, R., Hutchinson, R. B., Norton, R. H., and Lambert, D. L. 1972, *Ap. J.*, **172**, 89.
Beer, R., Norton, R. H., and Seaman, C. H. 1971, *Rev. Sci. Instr.*, **42**, 393.
Bernath, P. F., and Amano, T. 1982, *J. Molec. spectrosc.*, **95**, 359.
Blackwell, D. E., Petford, A. D., and Shallis, M. J. 1980, *Astr. Ap.*, **82**, 249.
Branch, D., Lambert, D. L., and Tomkin, J. 1980, *Ap. J. (Letters)*, **241**, L83.
Carlone, C., and Dalby, F. W. 1969, *Canadian J. Phys.*, **47**, 1945.
Cartwright, D. C., and Hay, P. J. 1982, *Ap. J.*, **257**, 383.
Chackerian, C., Jr., and Tipping, R. H. 1983, *J. Molec. Spectrosc.*, **99**, 431.
Chu, S.-I., Yoshimine, M., and Liu, B. 1974, *J. Chem. Phys.*, **61**, 5389.
Cloutman, L. D., and Whitaker, R. W. 1980, *Ap. J.*, **237**, 900.
Colket, M. B., III 1984, *J. Quant. Spectrosc. Rad. Transf.*, **31**, 7.
Das, G., Wahl, A. C., and Stevens, W. J. 1974, *J. Chem. Phys.*, **61**, 433.
Dyck, H. M., Lockwood, G. W., and Capps, R. W. 1974, *Ap. J.*, **189**, 89.
Eggen, O. J. 1973, *Pub. A.S.P.*, **85**, 289.
Engleman, R., and Rouse, P. E. 1975, *J. Quant. Spectrosc. Rad. Transf.*, **15**, 831.
Faÿ, T. D., and Johnson, H. R. 1973, *Ap. J.*, **181**, 851.
Faÿ, T. D., Stein, W. L., and Warren, W. H. 1973, in Proc. Conf. Red Giant Stars (Indiana: Astronomy Department), p. 147.
Geballe, T. R., Wollman, E. R., Lacy, J. H., and Rank, D. M. 1977, *Pub. A.S.P.*, **89**, 840.
Gillis, J. R., and Goldman, A. 1981, *J. Quant. Spectrosc. Rad. Transf.*, **26**, 23.
Goldberg, L., Hege, E. K., Hubbard, E. N., Strittmatter, P. A., and Cocke, W. J. 1982, in *Second Cambridge Workshop on Cool Stars, Stellar Systems, and the Sun*, ed. M. S. Giampapa and L. Golub (*Smithsonian Ap. Obs. Spec. Rept.*, No. 392), Vol. **1**, p. 131.
Goon, G., and Auman, J. R. 1970, *Ap. J.*, **161**, 533.
Graham, W. R. W., and Lew, H. 1978, *Canadian J. Phys.*, **56**, 85.
Gustafsson, B., Bell, R. A., Eriksson, K., and Nordlund, A. 1975, *Astr. Ap.*, **42**, 407.
Hall, D. N. B., Ridgway, S. T., Bell, R., and Yarborough, J. M. 1978, *Proc. Soc. Photo-Opt. Instrum. Eng.*, **172**, 121.
Harris, M. J., and Lambert, D. L. 1984, *Ap. J.*, **281**, 739.
Hayes, D. P. 1980, *Ap. J. (Letters)*, **241**, L65.
Hinkle, K. H., and Lambert, D. L. 1975, *M.N.R.A.S.*, **170**, 447.
Hinkle, K. H., Lambert, D. L., and Snell, R. L. 1976, *Ap. J.*, **210**, 684.
Hocking, W. H., Gerry, M. C. L., and Merer, A. J. 1979, *Canadian J. Phys.*, **57**, 54.
Holweger, H., and Müller, E. A. 1974, *Solar Phys.*, **39**, 19.
Humphreys, R. M. 1978, *Ap. J. Suppl.*, **38**, 29.
Humphreys, R. M., Strecker, D. W., and Ney, E. P. 1972, *Ap. J.*, **172**, 75.
Johnson, H. L. 1967, *Ap. J.*, **149**, 345.
Johnson, H. L., and Mendoza V., E. E. 1966, *Ann. d'Ap.*, **29**, 525.
Johnson, H. R., Bernat, A. P., and Krupp, B. M. 1980, *Ap. J. Suppl.*, **42**, 501.
Johnson, H. R., and Krupp, B. M. 1976, *Ap. J.*, **206**, 201.
Johnson, H. R., Mould, J. R., and Bernat, A. P. 1982, *Ap. J.*, **258**, 161.
Johnson, H. R., and Steinman-Cameron, T. Y. 1982, in *Second Cambridge Workshop on Cool Stars, Stellar Systems and the Sun*, ed. M. S. Giampapa and L. Golub (*Smithsonian Ap. Obs. Spec. Rept.*, No. 392), Vol. **I**, p. 239.
Jura, M., and Morris, M. 1981, *Ap. J.*, **251**, 181.
Kaler, J. B., Iben, I., and Becker, S.A. 1978, *Ap. J. (Letters)*, **224**, L63.
Kirby-Docken, K., and Liu, B. 1978, *Ap. J. Suppl.*, **36**, 359.
Kodaira, K., Tanka, W., Onaka, T., and Watanabe, T. 1979, *Pub. Astr. Soc. Japan*, **31**, 667.
Kurucz, R. L. 1970, *Smithsonian Ap. Obs. Spec. Rept.*, No. 309.
Lambert, D. L. 1974, *Highlights Astr.*, **3**, 237.
———. 1978, *M.N.R.A.S.*, **182**, 249.
Lambert, D. L., and Beer, R. 1972, *Ap. J.*, **177**, 541.
Lambert, D. L., Brooke, A. L., and Barnes, T. G. 1973, *Ap. J.*, **186**, 573.
Lamb, S. A., Iben, I., Jr., and Howard, W. M. 1976, *Ap. J.*, **207**, 209.
Larsson, M., Siegbahn, P. E. M., and Ågren, H. 1983, *Ap. J.*, **272**, 369.
Lee, T. A. 1970, *Ap. J.*, **162**, 217.
Luck, R. E. 1977, *Ap. J.*, **212**, 743.
———. 1979, *Ap. J.*, **232**, 797.
Luck, R. E., and Lambert, D. L. 1982, *Ap. J.*, **256**, 189.
Maillard, J. P., Chauville, J., and Mantz, A. W. 1976, *J. Molec. Spectrosc.*, **63**, 120.
Mauron, N., Fort, B., Querci, F., Dreux, M., Fauconnier, T., and Lamy, P. 1984, *Astr. Ap.*, **130**, 341.
Mies, F. H. 1974, *J. Molec. Spectrosc.*, **53**, 150.
Murphy, R. E. 1971, *J. Chem. Phys.*, **54**, 4852.
Norton, R. H., and Beer, R. 1976, *J. Opt. Soc. Am.*, **66**, 259.
Peytremann, E. 1974, *Astr. Ap.*, **33**, 203.
Phillips, J. G. 1973, *Ap. J. Suppl.*, **26**, 313.
Piccirillo, J., Bernat, A. P., and Johnson, H. R. 1981, *Ap. J.*, **246**, 246.
Podolske, J. R., and Johnston, H. S. 1983, *J. Chem. Phys.*, **79**, 3633.
Ridgway, S. T., Joyce, R. R., White, N. M., and Wing, R. F. 1980, *Ap. J.*, **235**, 129.
Roux, F., d'Incan, J., and Cerny, D. 1973, *Ap. J.*, **186**, 1141.
Sauval, A. J., Grevesse, N., Brault, J. W., Stokes, G. M., and Zander, R. 1984, *Ap. J.*, **282**, 330.

Schwarzschild, M. 1975, *Ap. J.*, **195**, 137.
Sneden, C., Johnson, H. R., and Krupp, B. M. 1976, *Ap. J.*, **204**, 281.
Sneden, C., and Lambert, D. L. 1982, *Ap. J.*, **259**, 381.
Spinrad, H., Kaplan, L. D., Connes, P., Connes, J., Knude, V. G., and Maillard, J. P. 1970, in *Proc. Conf. on Late-Type Stars*, ed. G. W. Lockwood and H. M. Dyck (*Kitt Peak Nat. Obs. Contr.*, No. 554), p. 59.
Spinrad, H., and Vardya, M. S. 1966, *Ap. J.*, **146**, 399.
Stevens, W. J. 1973, *J. Chem. Phys.*, **58**, 1264.
Stevens, W. J., Das, G., Wahl, A. C., Krauss, M., and Neumann, D. 1974, *J. Chem. Phys.*, **61**, 3686.
Stothers, R., and Chin, C.-W. 1977, *Ap. J.*, **211**, 189.
———. 1979, *Ap. J.*, **233**, 267.
Thompson, R. I. 1973, *Ap. J.*, **181**, 1039.
Tipping, R. H. 1976, *J. Molec. Spectrosc.*, **61**, 272.
Tsuji, T. 1976*a*, *Pub. Astr. Soc. Japan*, **28**, 543.
———. 1976*b*, *Pub. Astr. Soc. Japan*, **28**, 567.
Tsuji, T. 1978, *Pub. Astr. Soc. Japan*, **30**, 435.
———. 1979, *New Zealand J. Sci.*, **22**, 415.
———. 1981, *Astr. Ap.*, **99**, 48.
Vogt, S. S., Tull, R. G., and Kelton, P. K. 1978, *Appl. Optics*, **17**, 574.
Wahl, A. C., and Das, G. 1970, *Adv. Quantum Chem.*, **5**, 261.
Watanabe, T., and Kodaira, K. 1978, *Pub. Astr. Soc. Japan*, **30**, 21.
———. 1979, *Pub. Astr. Soc. Japan*, **31**, 61.
Werner, H.-J., Rosmus, P., and Reinsch, E.-A. 1983, *J. Chem. Phys.*, **79**, 905.
White, N. M. 1980, *Ap. J.*, **242**, 646.
White, N. M., and Wing, R. F. 1978, *Ap. J.*, **222**, 209.
Wilson, O. C. 1959, *Ap. J.*, **131**, 75.
———. 1976, *Ap. J.*, **205**, 823.
Wing, R. F. 1971, in *Proc. Conf. Late-Type Stars*, ed. G. W. Lockwood and H. M. Dyck (*Kitt Peak Nat. Obs.*, No. 554), p. 145.
Wing, R. F., and Spinrad, H. 1970, *Ap. J.*, **159**, 973.
Zetzsch, C. 1978, *Ber. Bunsenges. Phys. Chem.*, **82**, 639.

JEFFERY A. BROWN and DAVID L. LAMBERT: Department of Astronomy, The University of Texas, Austin, TX 78712

KENNETH H. HINKLE: Kitt Peak National Observatory, P.O. Box 26732, Tucson, AZ 85726

HOLLIS R. JOHNSON: Astronomy Department, Indiana University, Swain Hall West 319, Bloomington, IN 47401